Macromolecules
ARTICLE

Macromolecules **2010**, *43*, 1543–1550 **1543**
DOI: 10.1021/ma902403a

Dynamic Force Spectroscopy of Oppositely Charged Polyelectrolyte Brushes

Evan Spruijt,* Martien A. Cohen Stuart, and Jasper van der Gucht

Laboratory of Physical Chemistry and Colloid Science, Wageningen University, Dreijenplein 6, 6703 HB Wageningen, The Netherlands

Received October 29, 2009; Revised Manuscript Received January 3, 2010

ABSTRACT: Ion pairing is the main driving force in the formation of polyelectrolyte complexes, which find widespread use in micellar assemblies, drug carriers, and coatings. In this paper we examine the actual ion pairing forces in a polyelectrolyte complex between two oppositely charged polyelectrolyte brushes. Using colloidal probe AFM, we study the effect of salt on the strength of the model complex. We find a strong dependence of attractive force on salt concentration up to a critical salt concentration beyond which no attraction can be measured. By changing the salt concentration, the time allowed for formation of the complex, and the rate at which the complex is disrupted, we are able to measure the kinetics of complex formation and to estimate the ion pairing forces in equilibrium polyelectrolyte complexes. We use a kinetic model for the dynamics of complex disruption as a function of disruption rate to find a typical force of ion pairing in the complex. The model shows that our model polyelectrolyte complex behaves as a series of bonded ion pairs loaded as a zipper.

If you mix under the right conditions a solution of a positively charged polymer with one of a negatively charged polymer, phase separation occurs and a complex is formed. These complexes are often liquidlike, and they were named complex coacervates when they were first discovered by Bungenberg−de Jong.[1] Complex coacervates or polyelectrolyte complexes have interesting applications, such as drug carriers,[2−5] fat replacers,[6,7] and coatings,[8,9] but they are also interesting from a biological perspective. In both eukaryotic and prokaryotic cells DNA is packed into a small volume by small DNA-binding proteins. The electrostatic attraction between the oppositely charged macroions is one of the main driving forces for this DNA compaction.[10]

The two main driving forces for the formation of a complex coacervate are the Coulomb attraction (ion pairing) and the entropy increase due to counterion release. In addition, several other interactions can contribute to the final stability of a complex coacervate phase. These include the hydrophobic effect, hydrogen bonding, and hydration forces.

The first mean-field theory to describe this phenomenon was proposed by Overbeek and Voorn and includes the electrostatic interaction in the Debye−Hückel approximation and Flory−Huggins entropic terms for all components in solution.[11] This theory predicts coexistence of a dense coacervate phase with a dilute aqueous phase and the existence of a critical salt concentration above which no phase separation occurs. Later, this theory was extended by Nakajima and Sato to include some of the additional terms, such as hydrophobicity, by means of an interaction parameter χ.[12] Castelnovo and Joanny derived a theory for complex coacervation that includes correlation effects that they argue play an important role in the dense coacervate phases.[13] They also predict a critical salt concentration for coacervation. Kramarenko and Khokhlov included specific ion pairing energies in their model for the formation of block ionomer micelles.[14] They ignore, however, the formation of ion pairs between polyelectrolytes and monovalent counterions, and therefore they did not present the salt dependence of the aggregation.

*Corresponding author. E-mail: evan.spruijt@wur.nl.

Since the development of these models, most experimental reports on the coacervation phenomenon have been phenomenological. The stability of such complexes has been described in terms of mixing ratios and salt concentration, but no direct measurement of the forces that keep complex coacervates together has been reported.

Direct measurement of intermolecular forces has profited greatly form the introduction of the AFM. This technique has made the measurement of forces between all types of surfaces and molecules possible. Examples include depletion forces between hydrophobic colloids,[15] forces due to the electrical double layer of charged colloids,[16] attractive and repulsive Casimir forces,[17,18] and forces between complementary strands of DNA,[19,20] of covalent bonds,[21,22] of protein unfolding, and of interactions between ligand and receptor.[23] Forces induced by polyelectrolytes have been studied as well by AFM. Hugel et al. measured elasticity and desorption of single polyelectrolyte chains and found wormlike chain stretching until a rupture at 1.5 nN.[24] Gelbert et al. reported on the collapse of a covalently attached and relatively hydrophobic polyelectrolyte brush as a function of salt, pH, and compression.[25] They used analysis of the noise power spectral density to determine viscoelastic properties of a compressed polyelectrolyte brush and found that the brush is highly compressible close to the brush collapse. Johansson et al. measured interaction forces between polyelectrolyte multilayers and found adhesive forces, increasing with increasing contact time between the surfaces, for multilayers with an identical top layer.[26] This suggests diffusion of the chains across the interface, but no quantification of the obervations was carried out in order to determine the actual chain mobility. In addition to AFM, many SFA have been carried out on similarly charged polyelectrolyte brushes. Balastre et al. reported on the effect of chain length and salt concentration on the interactions between adsorbed polyelectrolyte brushes.[27] More recently, Dunlop et al. reported measurements of shear forces between covalently attached polyelectrolyte brushes.[28] Finally, optical tweezers have been used to measure forces of interaction between similarly charged polyelectrolyte-grafted surfaces.[29] Kegler et al. used a

Published on Web 01/13/2010

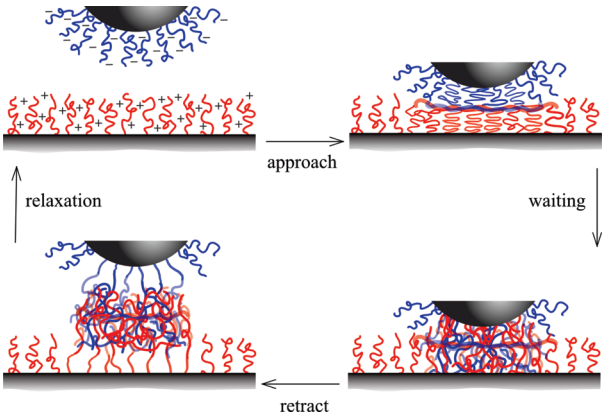

Figure 1. Artist's impression of the processes involved in dynamic force spectroscopy of oppositely charged polyelectrolyte brushes, showing approach of the surfaces (top), immediate complex formation upon first contact, interpenetration of chains and complex growth during a waiting step, stretching of the chains upon separation, and finally rupture of the complex before returning to the initial state.

biotin−streptavidin pair to link single strands of DNA to colloids and measured repulsive interactions of several piconewtons at a separation distance of 40 nm between the colloids, but they did not compress the brushes further. The group of Kremer reported on the interactions between pairs of weakly charged, negative poly(acrylic acid)-grafted colloids[30] and pairs of weakly charged, positive poly(2-vinylpyridine)-grafted colloids.[31] In both cases, they found that the repulsive interactions are dominated by entropic forces.

In this paper we use colloidal probe AFM to directly measure the forces between oppositely charged polyelectrolyte brushes. Colloidal probe AFM (CP-AFM), introduced independently by Ducker et al.[32] and by Butt,[33] provides a geometrically well-defined setup in which two surfaces can be brought into contact, as schematically shown in Figure 1. We recently applied this method to study the cohesive free energy in a complex coacervate phase of two oppositely charged polyelectrolytes by measuring capillary forces of the coacervate phase between two surfaces.[34] Here, we consider the same pair of polyelectrolytes, but now each covalently attached to its own surface, thus forming two oppositely charged brushes. We find that the critical salt concentration beyond which no interaction is measured is comparable to that of the situation where the polyelectrolytes are not covalently attached, but the attractive forces below the critical point are significantly larger in the grafted case. We ascribe these strong forces to the formation and rupture of ion pairs between the oppositely charged polyelectrolyte chains, as opposed to the interfacial energies associated with bringing neutral complexes together that have been measured in the ungrafted case. To describe the dynamics of ion pair formation and rupture, we carry out dynamic force spectroscopy measurements and we develop a kinetic model that describes our experimental data. We believe that such a quantitative approach to polyelectrolyte complex formation will lead to a better understanding of the stability and dynamics of these complexes.

Experimental Section

Materials. All chemicals are used as received from the manufacturer, unless stated otherwise. For the atom transfer radical polymerization (ATRP) of the polymer brushes, we use two types of monomers: METAC (2-(methacryloyloxy)ethyltrimethylammonium chloride), a positively charged monomer, and KSPM (potassium salt of 3-sulfopropyl methacrylate), a negatively charged monomer, both purchased from Aldrich. Inhibitor is removed from the METAC solution by running it through a neutral alumina column. The other chemicals used in the polymerization, 2,2′-dipyridyl (ligand), $CuCl_2$, CuCl, methanol, and isopropanol, are purchased from Aldrich as well. The polymerization is initiated by 3-trimethoxysilylpropyl-2-bromo-2-methylpropionate (silane initiator), which is purchased from Gelest Inc. (UK).[28] Deionized water with a resistance of 18.2 MΩ·cm is used.

Triangular AFM contact-mode cantilevers with actual spring constants of 0.08−0.50 N/m are purchased from Veeco. Silica probes (R = 3 μm) are a gift from Philips Laboratories. After modification, they are glued to the tip of a cantilever using a single-component, meltable epoxy glue. Flat silicon wafers with a 3 nm thick layer of native oxide, as determined by ellipsometry, are purchased from WaferNet.

Polyelectrolyte Brushes. Cationic PMETAC and anionic PSPM brushes are prepared on flat and spherical silica surfaces by surface-initiated aqueous ATRP. First, all surfaces are cleaned by rinsing with water and ethanol and subsequent plasma treatment for 2 min. Spherical silica particles are centrifuged at 10 000 rpm for 2 min between each rinsing step and sonicated during modification and rinsing steps. Both flat and spherical surfaces are modified with the silane initiator by placing them in a 5% (v/v) solution of silane initiator in hexane for 2 h, rinsing twice with hexane and twice with ethanol, and drying under a stream of N_2. The preparation of the polymerization solutions is described elsewhere in detail.[35−37] Briefly, for cationic PMETAC brushes a solution of [METAC]:[BiPy]:[CuCl]:[$CuCl_2$] = 100:4:2:0.1 in isopropanol:water (4:1) and a reaction time of 2 h was used, leading to brushes which are ∼50 nm thick when dry. For anionic brushes a solution of [KSPM]:[BiPy]:[CuCl]:[$CuCl_2$] = 75:1:0.2:0.1 in methanol:water (1:2) and a reaction time of 2 h are used, leading to ∼50 nm thick dry brushes as well. After the polymerization all surfaces are rinsed twice with water, twice with methanol and twice with ethanol. The spherical particles are washed five times with water and five times with methanol by subsequent sonication and centrifugation in order to remove all copper crystals, which is more difficult to remove because the particles tend to stick together. After washing, both flat and spherical surfaces are dried under a stream of N_2.

Dry and swollen brush thicknesses are measured by ellipsometry (Multiskop, Optel GBR), using an angle of incidence of 70 °C, a laser wavelength of 632.8 nm, and a two-layer model (substrate and brush layer) for fitting. We measure the thickness, L, and refractive index, n, of the brush layer at at least five independent locations on each sample. We find average dry brush thicknesses, L_{dry}, of ∼50 nm for the synthetic protocol described above, leading to 100−120 nm thick swollen brushes in pure water (see Supporting Information). The grafting density, σ, of these brushes is measured by cleaving off the brushes from a flat silicon wafer, according to a procedure described by Jones et al.,[38] and found to be 0.8 ± 0.3 nm^{-2} (see Supporting Information). We assume that brush thickness and grafting density on spherical surfaces are the same as on flat surfaces because the size of the spherical particles is large compared to the thickness of the brushes.

Force Spectroscopy. Force measurements are performed on a Nanoscope 4 AFM (Digital Instruments), equipped with a PicoForce scanner. Two surfaces with a polyelectrolyte brush are enclosed in a liquid cell with a volume of ∼250 μL, sealed by a rubber ring. The flat surface, modified with a PMETAC brush, is facing up, and the spherical particle, modified with a PSPM brush, is glued to the AFM tip using a meltable epoxy glue and facing down. The liquid cell is filled with a filtered solution of KCl in water, with concentrations varying from 0 to 3 M.

Force−distance curves are measured using a scan range of 500−2000 nm and scan rates ranging from 4 to 2000 nm/s. At least 20 separate force curves are recorded for every sample and every scan rate, except the lowest, for which 10 force curves are recorded. The increasing linear part of the force curve, i.e., in the

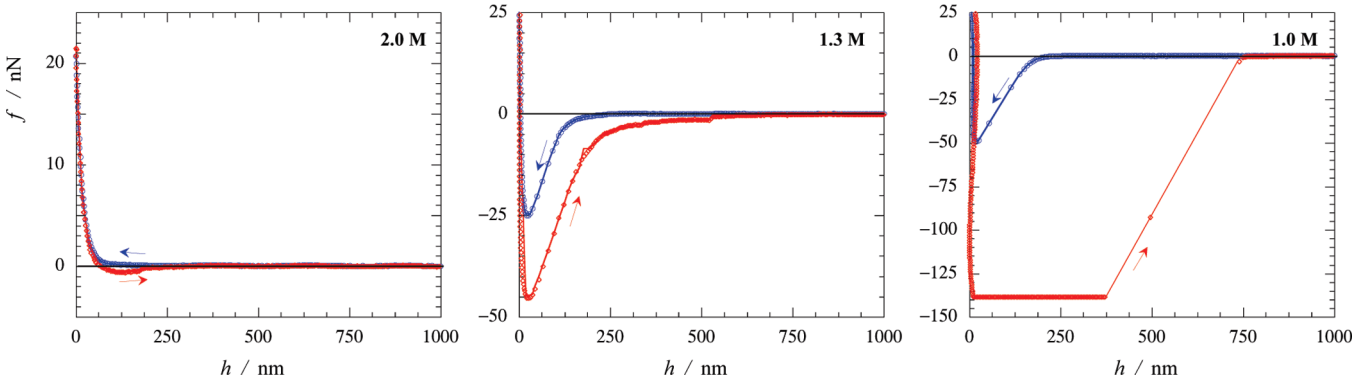

Figure 2. Typical force−distance curves between a negatively charged PSPM and a positively charged PMETAC brush at three different salt (KCl) concentrations as indicated by the labels. The curves show both approach and separation curves, as indicated by the arrows. All force curves are recorded with a scan rate of 2000 nm/s, a scan size of 2 μm, and a force trigger of +25 nN to start separation of the surfaces after approach.

constant compliance region, is taken as the distance of closest approach. At this separation distance, the two silica surfaces are not in contact due to the polyelectrolyte brushes that are sandwiched between the surfaces. The reference $h = 0$ will therefore refer to the separation distance at which the two polyelectrolyte brushes are compressed strongly, without relating this to an absolute separation distance between the silica surfaces. All other distances are derived from this reference position. The cantilever deflection data are converted to interaction forces using Hooke's law, $F = k\Delta z$, where k is the cantilever spring constant. In this study we use different cantilevers with spring constants in the range of 0.08−0.50 N/m to cover the range of attractive forces from very strong at low salt concentrations to very weak at high salt concentrations. Spring constants are determined for every cantilever separately using the thermal tuning method introduced by Hutter and Bechhoefer.[39]

Kinetic experiments are performed using AFM by applying a waiting step between the approach and separation cycle of the scanner head. During the waiting step the piezo attached to the cantilever is kept at a fixed position, which keeps the two surfaces in contact. A force trigger of 30 nN is used to define the start of the waiting step such that the brushes are compressed with a constant force during the waiting step. We checked that no significant drift of either position or force occurred during this waiting step.

Reproducibility. Reproducibility of our data is checked on two levels. First, in order to achieve good reproducibility of force measurements for different samples, all spherical silica particles we use are prepared in the same synthesis and checked under an optical microscope to be spherical and free from solid precipitates. Freshly prepared polyelectrolyte brushes on flat surfaces are always evaluated by ellipsometry, to measure thickness (L_{dry} = 50 ± 5 nm; n_{dry} = 1.47 ± 0.01), and by microscopy to make sure no solid residue is present on the flat surfaces either. This resulted in an estimated error in the measured attractive forces between different samples of less than 20%, based on a separate loading experiment with different surfaces (see Supporting Information).

Second, force curves for a single set of modified surfaces are found to be reproducible when experiments last for less than ~1 h. Force curves that are measured continuously for 2 h show a gradual decrease of the maximal attractive force (see Supporting Information). This decrease is attributed to erosion of the brushes, i.e., covalently grafted chains are being pulled out of the brushes. The erosion process is found to depend mainly on the salt concentration used in the experiments. On the basis of these considerations, all experiments of a single set of modified surfaces are carried out within 1 h.

Results and Discussion

Force−Distance Curves. Surfaces covered with oppositely charged polyelectrolyte brushes give rise to very strong attractive forces in AFM, much larger than recently reported for surfaces covered with an adsorbed polyelectrolyte (multi)layer, even though the colloidal probe dimensions are comparable.[26] For typical brushes we use in our experiments in aqueous solutions without added salt the attractive force becomes so strong that during separation of the two surfaces the glue connection between the colloidal probe and the AFM tip breaks first as the weakest link, instead of the noncovalent interactions between the oppositely charged brushes. Therefore, we always start our force measurements in an aqueous solution with a high salt concentration (2−3 M) and then gradually proceed to lower concentrations.

A typical series of force curves, starting at a high salt concentration and changing to lower salt concentrations, is shown in Figure 2. In solutions with a salt concentration of 2.0 M, no attractive force is measured upon approach, and only a very weak adhesion is measured when the surfaces are separated again. This weak adhesion force of 0.1−1 nN is measured for all brushes in solutions with a salt concentration in the range 2−3 M. In addition to the weak attractive force, we measure a repulsive force between the two brushes in both the approach and separation cycle of the force−distance curve for distances smaller than 50 nm. This repulsion of course results from mutual compression of the brushes.

In solutions with a lower salt concentration (1.3 M), we measure an attractive force in both the approach and separation curve. The hysteresis between approach and separation in both the strength of the attractive force and range of attraction suggests that a dynamic process is taking place in the time between first contact of the brushes upon approach and final release of the brushes upon separation. This process will be discussed in detail in the following sections. We note that the range of the attractive force is in agreement with the thickness of the swollen polyelectrolyte brushes that we use in these experiments. A repulsive force is not measured here until the constant compliance region is reached, due to the fact that attraction dominates until the brushes are strongly compressed, swamping the tail of the repulsive interaction.

In solutions with a salt concentration below 1.0 M, the attractive force in the separation curve has become too strong to be measured with our AFM. This is reflected in Figure 2c by a horizontal plateau at an attractive force that represents the detection limit of our AFM for this specific cantilever. Upon separation, the colloidal probe sticks to the facing flat surface and the cantilever bends as the piezo element moves the two surfaces apart. At a certain point, enough energy has been stored in the cantilever to disrupt the contact between the two brushes and the cantilever jumps back over a distance of 400 nm to an undeflected position.

Hysteresis in the force−distance curves originates from slow processes that occur once the brushes are brought into contact. Figure 1 gives a schematic overview of the different steps we believe take place during the measurement of one force−distance curve. When the brushes are approached, a complex is formed at the point where the brushes come in contact. This complex is a skinlike layer between the two brushes. Initially, the brushes on both sides of the skin layer are compressed in the final stage of the approach curve, but while the brushes are kept in contact, they start to interpenetrate. During an optional waiting step the interpenetration continues and the complex phase grows between the surfaces. Then, the surfaces are separated again and the polyelectrolyte chains are stretched until enough energy is stored to disrupt the complex phase. The detachment is of a catastrophic nature: once a few ion pairs within the polyelectrolyte are disrupted, the force is transferred to the remaining ion pairs which will be disrupted as well until the whole complex is disrupted. Now the brushes are completely separated again, and relaxation of the polyelectrolyte chains takes place.

On the basis of the picture sketched above, we expect that hysteresis in the force−distance curves can be minimized by reducing the scan rate of the piezo element while also reducing the time the brushes are compressed, i.e., beyond the point where the interaction turns repulsive, as much as possible. Using this approach, the waiting time in Figure 1 is minimized, and only a skin layer of complex is formed. In the limit of very low scan rates we should then approach a reversible (i.e., equilibrium) force curve.

Figure 3a shows a force−distance curve using the lowest scan rate accessible with our setup where interference from drift is not significant yet: 20 nm/s over a total scan range of 1000 nm. We reduce the compression time of the brushes to less than 50 ms. Upon approach of the two surfaces an attractive force is measured with a range of 200 nm. The attraction increases with decreasing distance between the surfaces because an increasing area of the two brushes comes into contact. At the point of contact between the brushes a complex is formed instantaneously. As we separate the brushes again after minor compression, we measure an almost identical attraction between the brushes with a range of attraction that is only slightly larger than in the approach curve. No sudden jumps of the tip occur, as shown in Figure 3b, where the actual tip velocity, derived as $v = \mathrm{d}h/\mathrm{d}t$ from Figure 3a, is plotted as a function of its position.

The fact that approach and separation interactions are almost identical suggests that we are indeed measuring a near-equilibrium process. For such processes the area under the curve in Figure 3a is a measure for the free energy of interaction of the skin layer of complex. Figure 3c shows how the energy of interaction, taken as the integral of the force−distance curve, changes as a function of the scan rate. The interaction energy of both the approach and the separation curve seem to level off to an equilibrium value for the free energy of interaction, which is estimated to be 5×10^{-16} J, based on power-law extrapolation of the data. We can estimate the number of contacts by approximating the contact area as $2\pi R\Delta h$,[40] where Δh is the range of interaction (~200 nm). This leads to an approximate number of contacts, n_0, of $2\sigma\pi R\Delta h = 3 \times 10^6$. We assume that on average one ion pair per contacting chain is formed in the skin layer of complex during such a short contact time and find an average free energy of interaction of $-0.04\ k_BT$ per ion pair for this particular salt concentration (1.4 M), close to the critical point. An important reason why the interaction energy of the approach scan and that of the separation curve will never be identical in this type of experiment is the fact that the polyelectrolyte brushes start to interpenetrate from the moment their outermost parts come in contact, which occurs already at a separation distance of 200 nm in the approach scan.

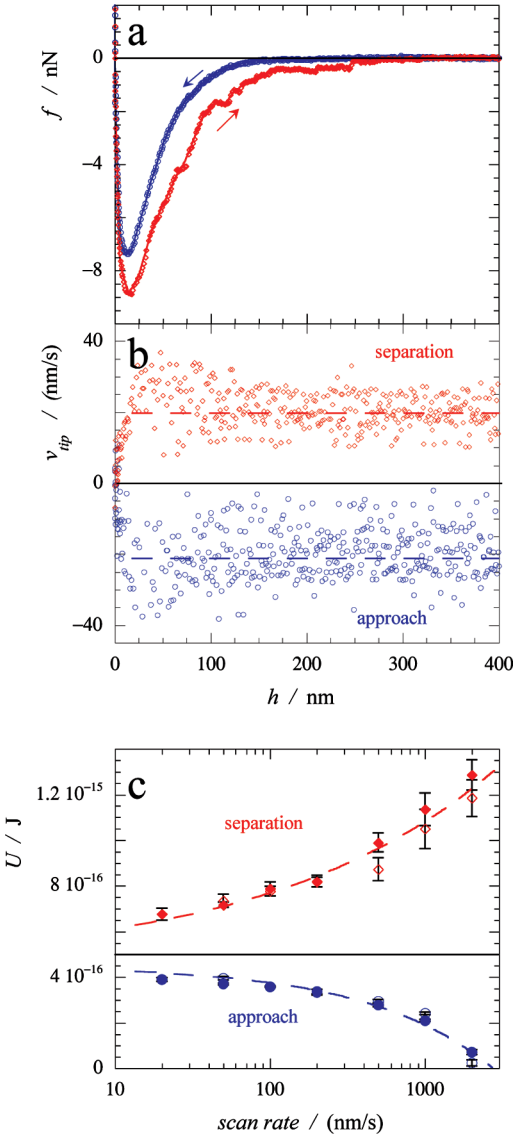

Figure 3. (a) Approaching a hysteresis-free force−distance curve between a PSPM and a PMETAC polyelectrolyte brush in solution with a salt concentration of 1.4 M KCl, by using a scan rate of 20 nm/s and a total time of compression (i.e., where repulsive forces are measured) of less than 50 ms. (b) Actual tip velocity as a function of separation of the two surfaces in the measurement shown in (a). Values for both approach and separation curve are shown. The dotted line is the input value for the scan rate. (c) Energy of interaction between a PSPM and PMETAC polyelectrolyte brush surface, approximated as the area under the force−distance curve, as a function of scan rate. Values based on both the approach and separation curve are shown. The dotted line is a power-law fit of the data according to $U = U_{eq} + av^b$, with identical U_{eq} of 5×10^{-16} J.

Effect of Salt on Polyelectrolyte Complex Strength. Qualitatively, we demonstrated in the previous section that salt has a strong effect on the interaction between oppositely charged polyelectrolyte brushes. Salt can be used to change the interaction from repulsive in solutions with a high salt concentration via reversibly attractive in solutions with an intermediate salt concentration to nearly irreversible sticking in solutions with no or a low salt concentration. Here we

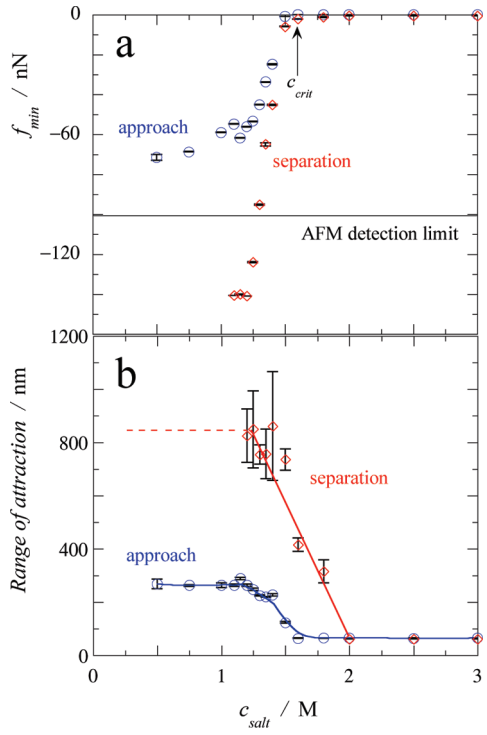

Figure 4. Effect of salt concentration on (a) the attractive force minimum and (b) the range of attraction in force−distance curves between a PSPM and a PMETAC polyelectrolyte brush. All corresponding force curves are recorded with a scan rate of 2000 nm/s, a scan size of 2 μm, and a force trigger of +25 nN to start separation of the surfaces after approach.

determine the value of the interaction force, the range of attraction, and the position of the attractive force minimum as a function of salt concentration.

Figure 4a shows the attractive force minimum for both approach and separation curves as a function of salt concentration for a fixed scan rate. We note that attraction between the surfaces is observed only below a critical salt concentration. In our experiments we find a critical salt concentration of 1.5 M, independent of scan rate. This critical salt concentration is comparable to the critical salt concentration found for polyelectrolyte complexes formed by nongrafted chains.[34] We explain this high critical salt concentration for both systems by a competition between monovalent salt ions and ionic groups on the polymer chains for the formation of ion pairs. When monovalent ions dominate, the polyelectrolyte complex becomes soluble and the attractive interaction between the two brushes vanishes. For monovalent ions to dominate in ion pair formation within the complex, the bulk salt concentration needs to be higher than the internal charge concentration in the complex phase. This internal charge concentration can be estimated from the transition between the osmotic and the salted brush regime. Ellipsometry measurements indicate that the internal salt concentration of our polyelectrolyte brushes is ~1.5 M (see Supporting Information).

Below the critical salt concentration we measure an attractive force that quickly becomes stronger with decreasing salt concentration. The hysteresis between approach and separation becomes larger with decreasing salt concentration as well. This indicates that the stronger contacts between the brushes slow down the kinetics of ion pair disruption (see Figure 1). For even lower salt concentrations the attractive forces upon separation of the brushes become stronger than the detection limit of our AFM (depending on the cantilever and set point).

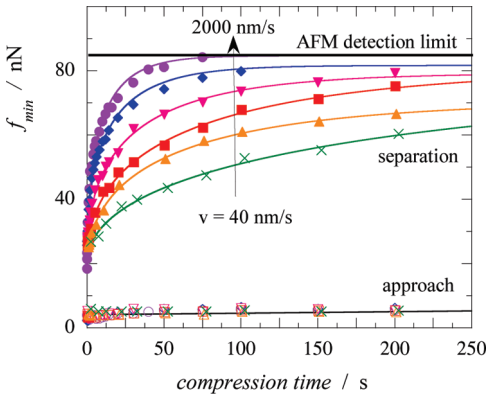

Figure 5. Attractive force minimum between a PSPM and a PMETAC brush as a function of compression time in solution with a salt concentration of 1.3 M for different scan rates. Each symbol corresponds to a different scan rates (in direction of the arrow): 40, 100, 200, 400, 1000, and 2000 nm/s. Values for both the approach and separation curves are shown. Solid lines for separation curves are drawn to guide the eye. All data points are recorded with a scan size of 2 μm and a constant compression force in contact of +30 nN.

Figure 4b shows the range of attraction, defined as the distance over which the attractive force is larger than 1 nN, as a function of salt concentration. Below the critical salt concentration the range of attraction increases with decreasing salt concentration. It reaches a plateau of ~300 nm for the approach. For the separation of the brushes, no correct range of attraction could be determined for force curves where a jump occurs, and only data for force curves lacking a jump out of contact are shown.

Finally, we measured the position of the attractive force minimum as a function of salt concentration (data not shown). We find that the position is not dependent on salt concentration and always occurs at distances smaller than 40 nm.

Kinetics of Complex Formation and Disruption. The slow dynamics of the polyelectrolyte chains precludes the measurement of a hysteresis-free force−distance curve and hence the determination of a true free energy of ion pairing without extrapolation. An alternative approach to determine the relevant interaction forces between the two oppositely charged polyelectrolyte brushes is therefore to take the dynamics explicitly into account. In dynamic force spectroscopy, kinetic processes are studied by changing the loading rate of the disruption process. In this paper, dynamic force spectroscopy is carried out for different compression times of the brushes in order to quantify the interpenetration of the brushes as schematically shown in Figure 1.

Figure 5 shows the dependence of the attractive force during approach and separation as a function of compression time for various scan rates. Upon approach of the brushes, no dependence of the attractive force on compression time is found, since the brushes have not yet been in contact. The measured rupture force upon separation, however, shows a clear increase with both increasing compression time and increasing scan rate.

In general, three possibilities exist for pulling apart two polymer chains that attract each other. If the separation proceeds via an equilibrium desorption process, no dependence of the rupture force on loading rate is expected.[41] If the separation process is dominated by friction between the sliding polymer chains, the rupture force is expected to scale linearly with the separation velocity, or loading rate, for a given compression time.[42] If the separation process is dominated by the kinetics of ion pair disruption (energetic contribution), the rupture force is expected to scale with the logarithm of the pulling velocity.[43,44]

On the basis of the results discussed in the previous section, we expect the kinetics of ion pair disruption to dominate the separation process. Moreover, the ion pairs can be formed along the entire polymer chain, and thus we expect the separation process to depend on the number of attachments per chain. A model that describes the dynamic force spectroscopy of multiple attachment points was derived by Evans and Ritchie[43] and Williams.[45] The derivation starts from the natural rate of dissociation (k_{off}) of a single attachment or connection. This dissociation rate increases by applying a force to the connection. We assume Kramer's type kinetics

$$k_d = \omega_0 \exp\left(-\frac{E_a - f x_{tr}}{k_B T}\right) = k_{off} \exp\left(\frac{f}{f_\beta}\right) \quad (1)$$

where $f_\beta = k_B T / x_{tr}$ sets the force scale and x_{tr} is the width of the potential well of the bond. The dissociation rate of N connections depends on the mechanism of loading. For parallel loaded connections, the force is shared equally between the connections and the force scale for these connections is multiplied by N. For connections loaded as a zipper, the force is transferred to a next connection after failure of the first bond, and therefore the force scale remains unchanged. We envision the separation of the complex formed between two polyelectrolyte brushes as the disruption of N ion pair connections loaded as a zipper. Then the failure of all N connections takes place at a rate of

$$k_d^{N \to 0} = \frac{1}{\tau_{tot}} = \left[\sum_{n=1}^{N} \frac{1}{k_{off}} \exp\left(-\frac{f}{f_\beta}\right)\right]^{-1} = \frac{1}{N} k_{off} \exp\left(\frac{f}{f_\beta}\right) \quad (2)$$

The second equality applies to N uncooperative bonds loaded as a zipper. The survival probability of the whole zipper can be calculated as

$$p(t) = \exp\left(-\int_0^t k_d[f(t')]\, dt'\right) \quad (3)$$

The average lifetime of the whole connection is now found by integrating over the survival probability: $t^* = \int_0^\infty p(t)\, dt$. For our AFM experiments, where we separate the surfaces with a constant velocity, the applied force increases linearly with time: $f = k_s v t$, where k_s is an effective spring constant of the chains that are being stretched. This leads to

$$t^* = \frac{f_\beta}{k_s v} \ln\left(\frac{k_s N v}{k_{off} f_\beta}\right) \quad (4)$$

and the total rupture force equals

$$f^* = n_0 k_s v t^* = n_0 f_\beta \ln\left(\frac{k_s}{k_{off} f_\beta}\right) + n_0 f_\beta \ln(N) + n_0 f_\beta \ln(v) \quad (5)$$

where n_0 is the total number of chains in contact.

Equation 5 predicts a logarithmic dependence of the rupture force on the scan rate. Figure 6 shows a plot of our experimentally determined rupture forces as a function of the logarithm of scan rate for varying contact times. These data are in perfect agreement with the zipper model.

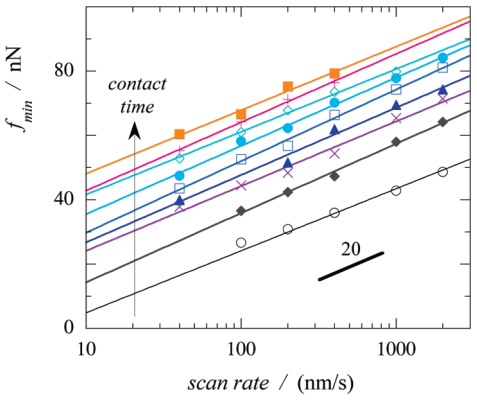

Figure 6. Dynamic force spectroscopy of two oppositely charged polyelectrolyte brushes (PSPM and PMETAC), showing the attractive force minimum as a function of scan rate in solution with a salt concentration of 1.3 M for different compression times. Each symbol corresponds to a different compression time (in direction of the arrow): 2, 10, 20, 30, 50, 75, 100, 150, and 200 s. Solid lines are fits to eq 5. All data points are recorded with a scan size of 2 μm and a constant compression force in contact of +30 nN.

The slope of the fits in Figure 6a is equal to $n_0 f_\beta \ln(10)$, so that, using the same estimate for the number of contacting chains as in the previous section, we find that the typical force of keeping ion pairs together at a salt concentration of 1.3 M is equal to 3 fN.

According to eq 5, the intercept of the fits in Figure 6 should increase as $\ln(N)$. It can be seen from the figure that the size of the complex, which is proportional to N, increases with increasing compression time. By plotting $f_{min} - n_0 f_\beta \ln(v)$ as a function of time, a mastercurve that is independent of scan rate should be found. This plot is shown in Figure 7a. Figure 7b shows a plot of $\exp[(f_{min}/n_0 f_\beta) - \ln(v)]$, which is directly proportional to the size of the complex, N, according to eq 5. The size of the complex is found to increase linearly with the compression time of the two brushes, indicating that the chains interpenetrate with a constant, but low velocity. In other words, the forces acting on every segment of the chain, such as the electrostatic interaction force driving complex growth and the friction force, slowing down growth of the complex, balance each other. We note that eventually the complex growth should slow down, when almost all charges along the polyelectrolyte chains are involved in ion pairs inside the complex, but this regime was not experimentally accessible.

At very short times we find that N deviates from the linear increase and has slightly larger values. This deviation is attributed to an underestimation of the total compression time of the brushes. The compression time has been estimated as the sum of the set delay time between approach and separation and the time during scanning where a repulsive force is measured in the constant compliance region. However, during approach of the brushes there is already contact between the outer parts of the brushes before a repulsive force is measured. Interpenetration of the brushes will already start there, thus leading to longer actual contact times. This systematic error is largest in Figure 7b for small set delays, i.e., at short total compression times.

Finally, we measure dynamic force spectroscopy at different salt concentrations to demonstrate the effect of salt on the interpenetration rate of the brushes. Figure 8 shows the growth of a complex phase at different salt concentrations, together with a logarithmic fit of the data, according to eq 5.

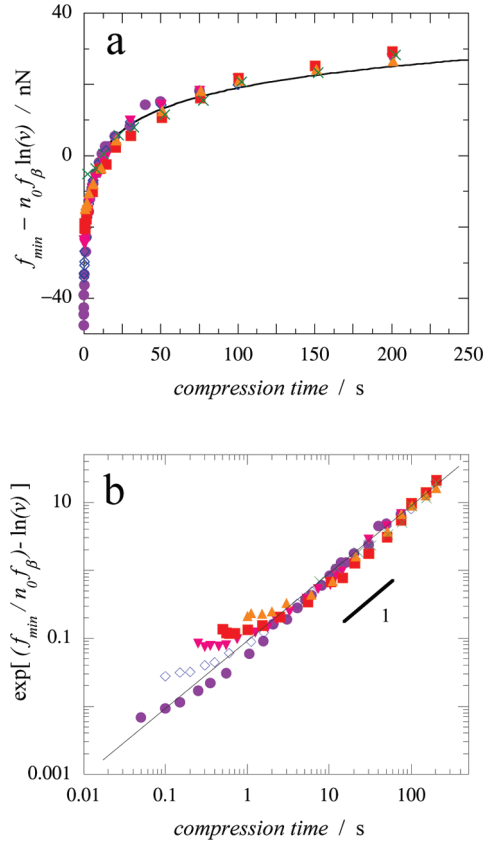

Figure 7. Rescaled attraction forces from dynamic force spectroscopy experiments as a function of compression time for the experiment described in Figure 5. Rescaling is carried out by (a) plotting $f_{min} - n_0 f_\beta \ln(v)$ as a function of compression time and (b) plotting $\exp[(f_{min}/n_0 f_\beta) - \ln(v)]$ as a function of compression time on a double-logarithmic scale. The solid line in (a) is a logarithmic fit to the combined data. The solid line in (b) is a power-law fit, with a slope of 1, to the combined data. Rescaled forces in (b) are directly proportional to the size of the complex phase (N).

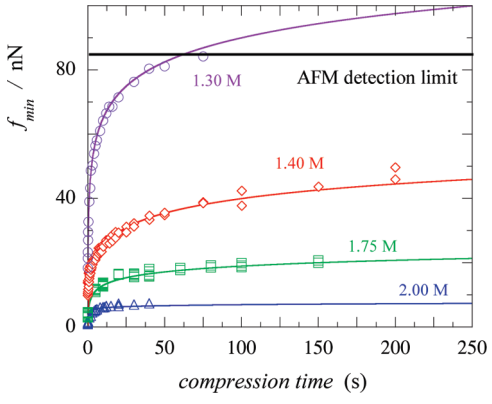

Figure 8. Dynamic force spectroscopy of two oppositely charged polyelectrolyte brushes: PSPM and PMETAC at different salt concentrations, as indicated by the labels. All data points are recorded with a scan rate of 2000 nm/s, a scan size of 2 μm, and a constant compression force in contact of +30 nN. Solid lines are logarithmic fits to the data.

We find not only significantly stronger forces at lower salt concentrations, but also a logarithmic dependence of f_{min} on t, suggesting that N increases linearly with t for all salt concentrations. The difference in slope for different salt concentrations is the result of different values for f_β, the typical force related to ion pairing, which is higher at lower salt concentrations.

Conclusions

We have described a direct way to measure the interaction forces responsible for stabilizing polyelectrolyte complexes in a model system consisting of two oppositely charged polyelectrolyte brushes in AFM. Because of the grafting of the chains with one end to a surface, the rupture process involves ion pair disruption and not adsorption and desorption processes of entire largely neutral complexes. We directly measure ion pair energies from very slow AFM scans and from dynamic force spectroscopy in combination with a kinetic model for the disruption of polyelectrolyte complexes. Our approach to directly measure such interactions in dense polyelectrolyte complexes is unique and allows for a better understanding of the formation and stability of such complexes. Understanding the interaction energies in polyelectrolyte complexes may help in designing improved complex coacervate coatings or polyelectrolyte complex-based drug carriers, where stability of the complexes is still an issue.

Acknowledgment. The authors thank Frans Leermakers for fruitful discussions. E.S. acknowledges financial support from The Netherlands Organisation for Scientific Research (NWO), project no. 021.002.013

Supporting Information Available: Experimental details. This material is available free of charge via the Internet at http://pubs.acs.org.

References and Notes

(1) de Jong, H. B.; Kruyt, H. *Proc. Sect. Sci., Koninklijke Nederlandse Akad. van Wetenschappen* **1929**, *32*, 849–856.
(2) Luzzi, L. *J. Pharm. Sci.* **1970**, *59*, 1367–1376.
(3) Thomasin, C.; Nam-Trân, H.; Merkle, H. P.; Gander, B. *J. Pharm. Sci.* **1998**, *87*, 259–268.
(4) Ohsugi, A.; Furukawa, H.; Kakugo, A.; Osada, Y.; Gong, J. P. *Macromol. Rapid Commun.* **2006**, *27*, 1242–1246.
(5) Voets, I. K.; de Keizer, A.; Cohen Stuart, M. A. *Adv. Colloid Interface Sci.* **2009**, *147−148*, 300–318.
(6) Bakker, M.; Konig, M.; Visser, J. World Patent Application WO94/14334, **1994**.
(7) Laneuville, S. I.; Paquin, P.; Turgeon, S. L. *J. Food Sci.* **2005**, *70*, s513–s519.
(8) Kester, J.; Fennema, O. *Food Technol.* **1986**, *40*, 47–59.
(9) de Vos, W. M.; Kleijn, J. M.; de Keizer, A.; Cohen Stuart, M. A. *Angew. Chem., Int. Ed.* **2009**, *48*, 5369–5371.
(10) Clark, D.; Kimura, T. *J. Mol. Biol.* **1990**, *211*, 883–896.
(11) Overbeek, J.; Voorn, M. J. *Cell. Comput. Phys.* **1957**, *49*, 7–26.
(12) Nakajima, A.; Sato, H. *Biopolymers* **1972**, *11*, 1345–1355.
(13) Castelnovo, M.; Joanny, J.-F. *Eur. Phys. J. E* **2001**, *6*, 377–386.
(14) Kramarenko, E. Y.; Khokhlov, A. R. *Polym. Sci. A* **2007**, *49*, 1053–1063.
(15) Milling, A.; Biggs, S. *J. Colloid Interface Sci.* **1995**, *170*, 604–606.
(16) Hu, K.; Fan, F.-R. F.; Bard, A. J.; Hillier, A. C. *J. Phys. Chem. B* **1997**, *101*, 8298–8303.
(17) Meurk, A.; Luckham, P. F.; Bergstrom, L. *Langmuir* **1997**, *13*, 3896–3899.
(18) Munday, J.; Capasso, F.; Parsegian, V. *Nature* **2009**, *457*, 170–173.
(19) Lee, G. U.; Chrisey, L. A.; Colton, R. J. *Science* **1994**, *266*, 771–773.
(20) Boland, T.; Ratner, B. D. *Proc. Natl. Acad. Sci. U.S.A.* **1995**, *92*, 5297–5301.
(21) Grandbois, M.; Beyer, M.; Rief, M.; Clausen-Schaumann, H.; Gaub, H. E. *Science* **1999**, *283*, 1727–1730.
(22) Garnier, L.; Gauthier-Manuel, B.; van der Vegte, E. W.; Snijders, J.; Hadziioannou, G. *J. Chem. Phys.* **2000**, *113*, 2497–2503.
(23) Zlatanova, J.; Lindsay, S. M.; Leuba, S. H. *Prog. Biophys. Mol. Biol.* **2000**, *74*, 37–61.
(24) Hugel, T.; Grosholz, M.; Clausen-Schaumann, H.; Pfau, A.; Gaub, H.; Seitz, M. *Macromolecules* **2001**, *34*, 1039–1047.
(25) Gelbert, M.; Biesalski, M.; Rühe, J.; Johannsmann, D. *Langmuir* **2000**, *16*, 5774–5784.
(26) Johansson, E.; Blomberg, E.; Lingström, R.; Wågberg, L. *Langmuir* **2009**, *25*, 2887–2894.

(27) Balastre, M.; Li, F.; Schorr, P.; Yang, J.; Mays, J. W.; Tirrell, M. V. *Macromolecules* **2002**, *35*, 9480–9486.
(28) Dunlop, I. E.; Briscoe, W. H.; Titmuss, S.; Jacobs, R. M.; Osborne, V. M.; Edmondson, S.; Huck, W. T.; Klein, J. *J. Phys. Chem. B* **2009**, *113*, 3947–3956.
(29) Kegler, K.; Salomo, M.; Kremer, F. *Phys. Rev. Lett.* **2007**, *98*, 058304.
(30) Dominguez Espinosa, G.; Synytska, A.; Drechsler, A.; Gutsche, C.; K., K.; Uhlmann, P.; Stamm, M.; Kremer, F. *Polymer* **2008**, *49*, 4802–4807.
(31) Elmahdy, M. M.; Synytska, A.; Drechsler, A.; Gutsche, C.; Uhlmann, P.; Stamm, M.; Kremer, F. *Macromolecules* **2009**, DOI 10.1021/ma901567d.
(32) Ducker, W. A.; Senden, T. J.; Pashley, R. M. *Nature* **1991**, *353*, 239–241.
(33) Butt, H.-J. *Biophys. J.* **1991**, *60*, 1438–1444.
(34) Spruijt, E.; Sprakel, J.; Cohen Stuart, M. A.; van der Gucht, J. *Soft Matter* **2010**, *6*, 172–178.
(35) Cheng, N.; Azzaroni, O.; Moya, S.; Huck, W. T. *Macromol. Rapid Commun.* **2006**, *27*, 1632–1636.
(36) Ramstedt, M.; Cheng, N.; Azzaroni, O.; Mossialos, D.; Mathieu, H.; Huck, W. *Langmuir* **2007**, *23*, 3314–3321.
(37) Spruijt, E.; Choi, E.-Y.; Huck, W. T. S. *Langmuir* **2008**, *24*, 11253–11260.
(38) Jones, D. M.; Brown, A. A.; Huck, W. T. S. *Langmuir* **2002**, *18*, 1265–1269.
(39) Hutter, J. L.; Bechhoefer, J. *Rev. Sci. Instrum.* **1993**, *64*, 1868–1873.
(40) Sprakel, J.; Bartscherer, E.; Hoffmann, G.; Cohen Stuart, M. A.; van der Gucht, J. *Phys. Rev. E* **2008**, *78*, 040802.
(41) Cui, S.; Liu, C.; Wang, Z.; Zhang, X.; Strandman, S.; Tenhu, H. *Macromolecules* **2004**, *37*, 946–953.
(42) Viovy, J.-L. *Rev. Mod. Phys.* **2000**, *72*, 813–860.
(43) Evans, E.; Ritchie, K. *Biophys. J.* **1997**, *72*, 1541–1555.
(44) Evans, E. *Annu. Rev. Biophys. Biomol. Struct.* **2001**, *30*, 105–128.
(45) Williams, P. *Anal. Chim. Acta* **2003**, *479*, 107–115.